IEEE Access
Multidisciplinary ⋮ Rapid Review ⋮ Open Access Journal

Received September 11, 2020, accepted September 21, 2020, date of publication September 25, 2020,
date of current version October 7, 2020.

Digital Object Identifier 10.1109/ACCESS.2020.3026749

Classification of Interference Signal for Automotive Radar Systems With Convolutional Neural Network

JINWOOK KIM[1], (Graduate Student Member, IEEE), SEONGWOOK LEE[2], (Member, IEEE), YONG-HWA KIM[3], (Member, IEEE), AND SEONG-CHEOL KIM[1], (Senior Member, IEEE)

[1]Department of Electrical and Computer Engineering, Seoul National University, Seoul 08826, South Korea
[2]School of Electronics and Information Engineering, College of Engineering, Korea Aerospace University, Goyang 10540, South Korea
[3]Department of Electronic Engineering, Myongji University, Yongin 17058, South Korea

Corresponding author: Yong-Hwa Kim (yongkim@mju.ac.kr)

This work was supported in part by the National Research Foundation of Korea (NRF) Grant funded by the Korean Government [Ministry of Science and ICT (Information & Communication Technology) (MSIT)] under Grant 2019R1A2C2086621, and in part by the Technology Innovation Program funded by the Ministry of Trade, Industry & Energy (MOTIE), South Korea (or Industrial Strategic Technology Development Program, Development of 77/79 GHz Dual Band Radar) under Grant 10080086.

ABSTRACT When a radar signal generated by another vehicle arrives at an ego-vehicle, mutual interference occurs, which can seriously degrade the detection performance of the radar. To mitigate mutual interference, the type of radar modulation used in the interference vehicle must be identified because the types of radar systems installed in each vehicle are different. Therefore, in this paper, we propose a method for classifying the modulation types of interference signals in automotive fast chirp frequency modulated continuous waveform (FMCW) radar systems. We build a mathematical model of the received signal when the radar signal transmitted by the ego-vehicle interferes with various types of interference signals, such as unmodulated continuous wave (CW), slow chirp FMCW, fast chirp FMCW, pulsed CW, and frequency-shift keying signals. In the fast chirp FMCW radar systems, the received signal is converted into range-Doppler response using two-dimensional Fourier transform. Based on range-Doppler responses of the interference signals, we design a classifier to identify the modulation type of interference signals using a convolutional neural network (CNN). Through our proposed CNN, we can classify five different types of interference signals with an accuracy of over 96%. In addition, compared to conventional feature-based machine learning techniques such as support vector machines, the proposed method can effectively identify the interference signal with fewer input signals in shorter time.

INDEX TERMS Automotive radar, modulation type classification, mutual interference, convolutional neural network (CNN).

I. INTRODUCTION

As interest in autonomous driving has recently increased, the use of radar sensors in vehicles has become mandatory [1] because the radar sensor is resistant to environmental changes and has a long detectable range compared to other automotive sensors, such as camera and sonar sensors [2]. If two or more radars share the same frequency band, mutual interference between these sensors can occur. Furthermore, as the number of vehicles equipped with radar sensors increases, the mutual interference can seriously degrade the detection performance of the radar [3]. Thus, to ensure a stable detection performance, it is essential to identify in advance what type of interference occurred and to apply an appropriate interference suppression technique. Several studies have proposed to mitigate interference signals generated between specific radar systems [4]–[6]. The authors in [4] proposed interference mitigation scheme which dealt with interference signal caused by two frequency modulated continuous waveform (FMCW) radars. They reconstructed interference signals using the wavelet denoising method and subtracted it from the low-pass filtered output signal. In [5], a method was proposed to mitigate the interference signal generated between fast chirp FMCW radars. The Kalman filter was used

The associate editor coordinating the review of this manuscript and approving it for publication was Shadi Alawneh.

to restore signals in the interference region by using signals from the non-interference region. The authors in [6] considered the case where FMCW radar signals interfered with continuous wave (CW) radar signals. With morphological component analysis, they separated interference signals into interference component and received beat signals. Therefore, if we identify the modulation type of interference, we can choose the appropriate interference mitigation method. However, since different manufacturers use different modulation schemes, it is very difficult to predict the interference pattern. Therefore, we need an effective method to identify the type of interference.

Several studies focusing on interference recognition have been conducted [7]–[9]. In [7], the authors proposed a method for classifying interference signals using Gini's coefficient. However, they only classified the modulation type of radar signals transmitted from other vehicles and did not consider the signals transmitted from the ego-radar system. The authors in [8] considered the case where a signal of the ego-radar system was received together with a signal of another radar. They suggested a classification model using a support vector machine (SVM). The frequency responses of received signals were used as input data for the model. However, they did not classify the frequency responses by extracting features from them; they instead used the magnitude of each frequency bin as input features. Therefore, it seems that this classification process requires considerable computation. The authors in [9] extracted features based on the statistical characteristics of the radar signal and used SVM to determine the modulation type of signal that interfered with the received signal. However, this model required full chirp data for feature extraction resulting in a time delay in the classification.

In this study, we propose an effective method for classifying the modulation type of interference signal in automotive radar systems. First, we formulate a mathematical model of the received signal when the fast chirp FMCW signal from the ego-vehicle's radar system is interfered with a signal from another interference vehicle's radar system. Five different modulation types of interference signals were considered in our work: unmodulated CW, slow chirp FMCW, fast chirp FMCW, pulsed CW, and frequency-shift keying (FSK) signals. In the fast chirp FMCW radar system, mutual interference can be effectively analyzed in two axes of slow-time and fast-time, which can be regarded as two-dimensional (2D) data. These 2D data, radar signals with interference, were transformed into a range-Doppler response by utilizing 2D Fourier transform. Thus, we propose a model using a convolutional neural network (CNN) which is effective for the 2D radar data. Recently, CNN's have been actively used in combinations with radar sensor data to classify target types [10]–[12] or specific actions [10], [13]. In this study, we proposed a CNN model composed of convolutional layers, fully connected layers, and an output layer, considering batch normalization and max pooling for better performance.

In simulation results, the proposed CNN-based method can classify five different interference signals with an accuracy of over 96% and it shows better classification accuracy than SVM's used in [8], [9]. Unlike feature-based machine learning techniques, our proposed method does not require hand-crafted features based on domain knowledge. In addition, whereas the conventional method requires the entire chirp data for classification, the proposed method allows classification using only a few chirps. This is to make faster decisions by lowering the amount of computation in generating input data of the CNN model. We took chirp data from the first column and transformed it into 2D range-Doppler response. The proposed algorithm showed 96.5% accuracy even when only 1% of the total chirps were used. We verified that the accuracy increased as the number of chirps used increased. We also compared the classification performance with the methods proposed in [8], [9].

The remainder of this paper is organized as follows. First, we describe the mathematical model of the received signal with interference signals in Section II. In Section III, the proposed CNN-based classification method is presented, including the input type and the framework for the CNN. Then, the classification results using the CNN are given in Section IV. Additionally, we also compare the performance of the proposed method to other classification methods. Finally, we conclude this paper in Section V.

II. RANGE-DOPPLER RESPONSE OF INTERFERENCE SIGNALS IN AUTOMOTIVE RADAR SYSTEMS

In automotive radar systems, if two or more radar-equipped vehicles share the same frequency band, mutual interference signals are generated. These signals contain frequency information about both the target and the interference sources. Therefore, by using the frequency information about the interference source, we can estimate its modulation type. In this section, mathematical models for the modulation types of the received interference signals are derived in range-Doppler response forms using 2D Fourier transforms.

A. FAST CHIRP FMCW RADAR SYSTEMS

We assume that the ego-vehicle transmits fast chirp FMCW radar signals for target detection. The fast chirp FMCW radar has an advantage over the conventional FMCW radar in terms of efficiency of target estimation. In the case of conventional systems, a target pairing process is necessary for target estimation. In multi-target situations, the pairing process can be a time-consuming task. In contrast, in the fast chirp FMCW radar system, the target estimation can be done without the target pairing process because the peaks corresponding to the targets appear in the 2D range-Doppler response [14]. For this reason, the fast chirp FMCW is the most widely used automotive radar system for autonomous driving. Fig. 1 shows this system, in which a transmitting antenna transmits a chirp signal whose frequency increases linearly with time. The transmitter repeatedly sends M chirps

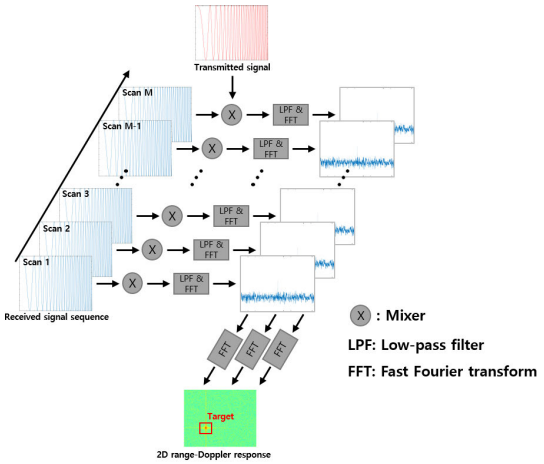

FIGURE 1. Radar signal processing in fast chirp FMCW radar systems.

and the corresponding transmitted signal can be expressed as

$$S_{TX}(t,\ m) = A_T \exp\left(j2\pi\left(\left(f_c - \frac{BW}{2}\right)t + \frac{BW}{2\Delta T}t^2\right) + j\phi_T\right) \quad (0 \le t < \Delta T,\ 0 \le m < M), \tag{1}$$

where A_T is the amplitude of the transmitted signal, f_c is the carrier frequency of the radar, BW is the bandwidth, ΔT is the sweep time of a chirp, t is the time value in the fast-time axis, m is the chirp index, and ϕ_T is the initial phase of the transmitted signal. A receiver receives these M chirps signals that are reflected from a target. The corresponding phase of the received signal can be expressed as

$$\phi_{RX}(t,\ m) = \left(f_c - \frac{BW}{2} + f_D\right)(t - t_d) + \frac{BW}{2\Delta T}(t - t_d)^2 \quad (t_d \le t < \Delta T,\ 0 \le m < M). \tag{2}$$

Compared to (1), there are phase differences in (2), which are caused by the target motion. The first one is from the Doppler shift f_D, which can be expressed as $\frac{2f_c v}{c}$. This is caused by the relative velocity v between the radar and the target. The second one is from the round-trip delay $t_d = \frac{2R(m)}{c}$, where t_d is the time delay for the transmitted signal to reach the target and return to the receiver and $R(m)$ is the distance between the radar and the target. Here, $R(m)$ is the distance for the mth chirp which can be expressed as $R+mv\Delta T$, where R is the initial range. This is because the radar and the target move with relative velocity v, which causes the range offset from the initial range R.

The received signals are then multiplied with the transmitted signal in a mixer to obtain a signal at the intermediate frequency. Higher frequency components are filtered with the low-pass filter. The corresponding phase of the mixer output signal can be expressed as

$$\phi_{MX}(t,\ m) = -f_D t + f_c t_d - \frac{BW}{2}t_d + f_D t_d + \frac{BW}{\Delta T}t t_d - \frac{BW}{2\Delta T}{t_d}^2 \quad (t_d \le t < \Delta T,\ 0 \le m < M). \tag{3}$$

The first, third, fourth, and last terms, which are expressed as $f_D t$, $\frac{BW}{2}t_d$, $f_D t_d$, and $\frac{BW}{2\Delta T}{t_d}^2$, respectively, can be neglected because they are relatively smaller than the other terms. Considering that $f_D = \frac{2f_c v}{c}$ and $t_d = \frac{2(R+mv\Delta T)}{c}$, $\phi_{MX}(t,\ m)$ can be approximated as

$$\phi_{MX}(t,\ m) \approx \frac{2f_c R}{c} + \frac{2f_c v\Delta T}{c}m + \frac{2BWR}{\Delta Tc}t + \frac{2BWvm}{c}t \quad (t_d \le t < \Delta T,\ 0 \le m < M). \tag{4}$$

Again, the last term $\frac{2BWvm}{c}t$ can be neglected because it is relatively smaller than the other terms. Finally, $\phi_{MX}(t,\ m)$ can be approximated as

$$\phi_{MX}(t,\ m) \approx \frac{2f_c R}{c} + \frac{2f_c v\Delta T}{c}m + \frac{2BWR}{\Delta Tc}t \quad (t_d \le t < \Delta T,\ 0 \le m < M). \tag{5}$$

Each chirp signal is sampled by an analog-to-digital converter (ADC) and N is the number of samples in a single chirp. Thus, the mixer output is defined in a $N \times M$ matrix form as

$$\mathbf{S} = [\boldsymbol{s}_c(1),\ \boldsymbol{s}_c(2),\ \cdots,\ \boldsymbol{s}_c(M)], \tag{6}$$

where $\boldsymbol{s}_c(m) = [s(1,\ m), \cdots, s(N,\ m)]^T$ and $s(n,\ m)$ is defined as

$$s(n,\ m) = A_M \exp\left(j2\pi\left(\frac{2f_c R}{c} + \frac{2f_c v}{c}\Delta Tm + \frac{2BWR}{\Delta Tc}\frac{\Delta T}{N}n\right) + j\phi_s\right). \tag{7}$$

In (7), A_M is the amplitude of the mixer output signal and ϕ_s is the phase offset.

When applying 2D Fourier transform on $\mathbf{S}$ in (6), we can estimate the target's velocity and range simultaneously. The resulting frequency response is called the range-Doppler response. The 2D Fourier transform can be performed step by step; for example, a column-wise Fourier transform can be performed first, followed by a row-wise Fourier transform. When column-wise Fourier transform is applied on the signal matrix $\mathbf{S}$, a peak appears at a specific frequency which corresponds to the last term in (7), $\frac{2BWR}{\Delta Tc}$. Therefore, this frequency implies the distance between the radar and the target. The corresponding frequency responses can be expressed in a $N_c \times M$ matrix form, where N_c is the number of points in the column-wise Fourier transform, as

$$\mathbf{X}_c = [\boldsymbol{x}_c(1),\ \boldsymbol{x}_c(2),\ \cdots,\boldsymbol{x}_c(M)], \tag{8}$$

here $\boldsymbol{x}_c(m) = [x(1, m), \cdots, x(N_c, m)]^T$ and $x(n_c, m)$ is defined as

$$x(n_c, m) = \sum_{n=1}^{N} s(n, m)\exp\left(-j\frac{2\pi n}{N_c}n_c\right). \tag{9}$$

Here, $\boldsymbol{x}_c(m)$ is the frequency response of $\boldsymbol{s}_c(m)$ and $\mathbf{X}_c$ is the frequency response following the column-wise Fourier transform.

Next, in (8), we apply Fourier transform on each row vector $\boldsymbol{x}_{cr}(n_c)$ in $\mathbf{X}_c$, where $\boldsymbol{x}_{cr}(n_c)$ is defined as $\boldsymbol{x}_{cr}(n_c) = [x(n_c, 1), \cdots, x(n_c, M)]$. The range-Doppler response can be expressed in a $N_c \times N_r$ matrix form, where N_r is the number of points in the row-wise Fourier transform, as

$$\mathbf{X}_{rv} = \begin{bmatrix} \boldsymbol{x}_{rv}(1) \\ \boldsymbol{x}_{rv}(2) \\ \vdots \\ \boldsymbol{x}_{rv}(N_c) \end{bmatrix}, \tag{10}$$

where $\boldsymbol{x}_{rv}(n_c) = [x_{rv}(n_c, 1), \cdots, x_{rv}(n_c, N_r)]$ is the frequency response of $\boldsymbol{x}_{cr}(n_c)$ and $x_{rv}(n_c, n_r)$ is defined as

$$x_{rv}(n_c, n_r) = \sum_{m=1}^{M} x(n_c, m) \exp\left(-j\frac{2\pi m}{N_r} n_r\right). \tag{11}$$

Fig. 2(a) shows the result of the column-wise Fourier transform when a single target moves at a speed of 20 m/s at a distance of 15 m. As shown in the figure, peaks are generated at 15 m in every column. In addition, a relative velocity between radar and target can be obtained when applying Fourier transforms on each row of $\mathbf{S}$. As shown in Fig. 2(b), peaks appear at the frequency of $\frac{2f_c v}{c}$, which is the second term in (7). Therefore, we can estimate that the target moves at a speed of 15 m/s.

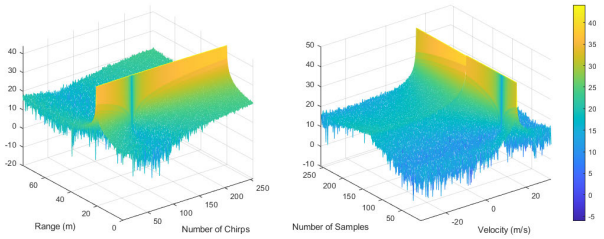

FIGURE 2. Frequency responses of fast chirp FMCW radar system (a) after column-wise Fourier transform (b) after row-wise Fourier transform.

Fig. 3 shows a range-Doppler response of the signal received from the target we set above. As shown in the figure,

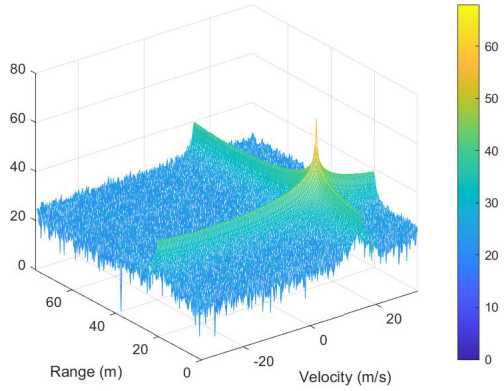

FIGURE 3. Range-Doppler response of fast chirp FMCW radar system: a peak corresponding to target appears at $(R, v) = (20\text{ m}, 15\text{ m/s})$.

peaks appear at certain values on the range and velocity axis, enabling the estimation of the target information as $R = 20$ m and $v = 15$ m/s. Furthermore, if two or more targets exist, the corresponding peaks appear at the range-Doppler response. Therefore, we can simultaneously estimate both the range and velocity of each target.

B. RANGE-DOPPLER RESPONSE OF THE INTERFERENCE SIGNAL

When some objects other than targets are nearby, their corresponding frequency responses appear at the range-Doppler response. Particularly, if there is an interference vehicle that also transmits radar signals for target detection, it acts as a new signal source, making frequency responses different from the target's frequency response. In this study, the simulation setup was based on three vehicles driving on a road as shown in Fig. 4. The blue car is an ego-vehicle equipped with a radar sensor and is capable of detecting other cars, the green car is a target vehicle driving in front of the detection vehicle, and the orange car is an interference vehicle that also emits radar signal for target detection and interferes with the ego-vehicle. The two radar-equipped vehicles share frequency bands; therefore, interference occurs.

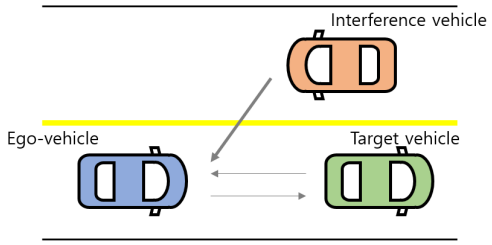

FIGURE 4. Driving environment.

We set five different modulations for the interference signal: the unmodulated CW, slow chirp FMCW, fast chirp FMCW, pulsed CW, and FSK signals. In [9], the mathematical expressions of the interference signals are presented when a fast chirp FMCW radar is used for target detection. The expressions are shown in Table 1.

All signals listed in Table 1 are the outputs of the mixer. As these signals are given in the form of a vector with a single time index, they must be converted into a matrix form of size $N \times M$ to check the range-Doppler responses, as shown in (6). The NM data samples sampled in the ADC are converted to the matrix form of (6), and then the range-Doppler response is obtained through the processes of (8)-(11). Analyzing the magnitude of range-Doppler responses, as presented in Fig. 5, we observe that different patterns are generated according to the modulation types. Fig. 5(a) and Fig. 5(b)-(f) show the magnitude of range-Doppler responses when only the target exists and when five different types of interference signals are received together, respectively. From the expressions in Table 1, different frequency components of the interference signals create specific patterns in range-Doppler responses. Therefore, we can expect that a deep learning model trained

TABLE 1. Modulation types of interference signals and mixer output signals.

Modulation of interference	Frequency	Mixer output signal
Unmodulated CW	constant with time	$S_{UC}(t) = A_{UC}\exp\left(j2\pi\left(\left(f_c - f_{cI} - f_D - \frac{BW}{2} - mBW\right)t + (f_{cI} + f_D)t_d + \frac{BW}{2\Delta T}t^2\right) + j\phi_{UC}\right)$ (12)
Slow chirp FMCW	linearly increase and decrease with time	$S_{SC}(t) = A_{SC}\exp\left(j2\pi\left(\left(f_c - f_{cI} - f_D - \frac{BW}{2} + (-1)^{n_s}\frac{BW_I}{2} - mBW + (-1)^{n_s}n_s BW_I + (-1)^{n_s}\frac{BW_I}{\Delta T_I}t_d\right)t + \frac{1}{2}\left(\frac{BW}{\Delta T} - (-1)^{n_s}\frac{BW_I}{\Delta T_I}\right)t^2 + \left(f_{cI} + f_D - (-1)^{n_s}\frac{BW_I}{2} - (-1)^{n_s}n_s BW_I\right)t_d - (-1)^{n_s}\frac{BW_I}{2\Delta T_I}t_d^2\right) + j\phi_{SC}\right)$ (13)
Fast chirp FMCW	linearly increase with short time	$S_{FC}(t) = A_{FC}\exp\left(j2\pi\left(\left(f_c - f_{cI} - f_D - \frac{BW}{2} + \frac{BW_I}{2} - mBW + n_I BW_I + \frac{BW_I}{\Delta T_I}t_d\right)t + \frac{1}{2}\left(\frac{BW}{\Delta T} - \frac{BW_I}{\Delta T_I}\right)t^2 + \left(f_{cI} + f_D - \frac{BW_I}{2} - n_I BW_I\right)t_d - \frac{BW_I}{2\Delta T_I}t_d^2\right) + j\phi_{FC}\right)$ (14)
Pulsed CW	constant frequency in short time	$S_{PC}(t) = A_{PC}\exp\left(j2\pi\left(\left(f_c - \sum_{n_P=0}^{N_P-1} f_{cI}\,\mathrm{rect}\left(\frac{t-n_P T_{PRI}}{T_P}\right) - f_D - \frac{BW}{2} - mBW\right)t + \frac{BW}{2\Delta T}t^2 + \left(\sum_{n_P=0}^{N_P-1} f_c\,\mathrm{rect}\left(\frac{t-n_P T_{PRI}}{T_P}\right) + f_D\right)t_d\right) + j\phi_{PC}\right)$ (15)
Frequency shift keying	vary with discrete value	$S_{FSK}(t) = A_{FSK}\exp\left(j2\pi\left(\left(f_c - f_{cI} - f_D - \frac{BW}{2} - mBW + f_{step}\frac{N_{step}-1-2(n_F \bmod N_{step})}{2}\right)t + \frac{BW}{2\Delta T}t^2 + \left(f_{cI} + f_D - f_{step}\frac{N_{step}-1-2(n_F \bmod N_{step})}{2}\right)t_d\right) + j\phi_{FSK}\right)$ (16)

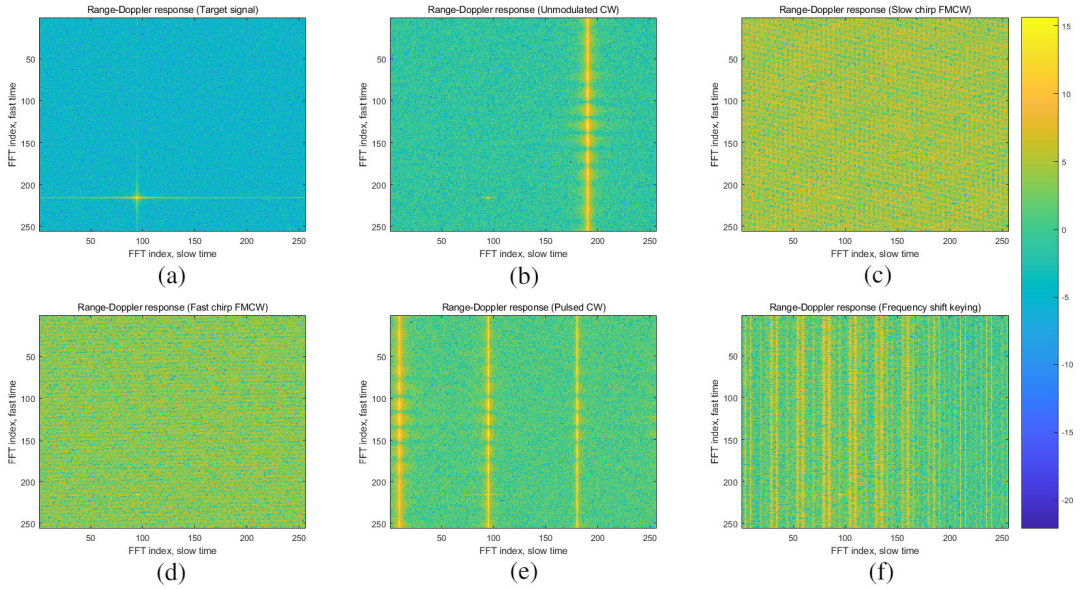

FIGURE 5. Range-Doppler responses of recevied signals when (a) only target signal, (b) unmodulated CW signal, (c) slow chirp FMCW signal, (d) fast chirp FMCW signal, (e) pulsed CW signal, and (f) FSK signal received.

with the magnitude of these frequency responses can ensure the identification of the interference signals.

III. PROPOSED METHOD

A. INPUT FORMAT

To classify the modulation types of interference signals, we consider a CNN model. Compared to an artificial neural network, the CNN employed convolution operations for learning, resulting a reduction in the number of training parameters and effective extraction of the local characteristics of the input image [15].

For the classification task, we use the magnitudes of range-Doppler responses $\mathbf{X}_{rv}$. First, these magnitudes are normalized to values from 0 to 1. When the maximum and

minimum values of $x_{rv}(n_c, n_r)$ in all data set are x_{rv}^{max} and x_{rv}^{min}, respectively, the normalized value $x_{rv}^{norm}(n_c, n_r)$ can be expressed as

$$x_{rv}^{norm}(n_c, n_r) = \frac{x_{rv}(n_c, n_r) - x_{rv}^{min}}{x_{rv}^{max} - x_{rv}^{min}}. \tag{17}$$

Thus, the normalized range-Doppler magnitude responses are defined in a matrix form as $\mathbf{X}_k^{in}$, where k is the index for the modulations of interference signals and the size of $\mathbf{X}_k^{in}$ is $N_c \times N_r$. We use $\mathbf{X}_k^{in}$ as the input of the CNN model for the interference classification. In this study, we set the number of points in the Fourier transforms equal to the number of time-domain data. Therefore, the size of the received signal matrix in the time-domain remains the same after 2D Fourier transform.

B. CNN MODEL

Fig. 6 shows the structure of our CNN model, which consists of a combination of convolutional layers, batch normalization layers, rectified linear unit (ReLU) activation layers, max pooling layers, fully connected layers, dropout layers, and an output layer. The detailed description of each layer is listed in Table 2. Each convolutional layer performs 5×5 convolution operations, and the number of filters increases as the layer becomes deeper. Both the stride and padding size are set to 2 in each convolutional layer. After convolution, the batch normalization is used to normalize the intermediate results of the model. With the batch normalization, the training speed can be improved because a gradient vanishing or gradient exploding can be prevented [16]. Then, we use the ReLU activation function [17], which is defined as

$$f(z^l) = \max\{0, z^l\} = \begin{cases} z^l, & z^l \geq 0 \\ 0, & \text{else} \end{cases} \tag{18}$$

where z^l is an element of outputs in lth convolutional layer. The max pooling layer is used to decrease the spatial size of features and parameters of the network [18]. The units in the final max pooling layer are flattened into a single vector.

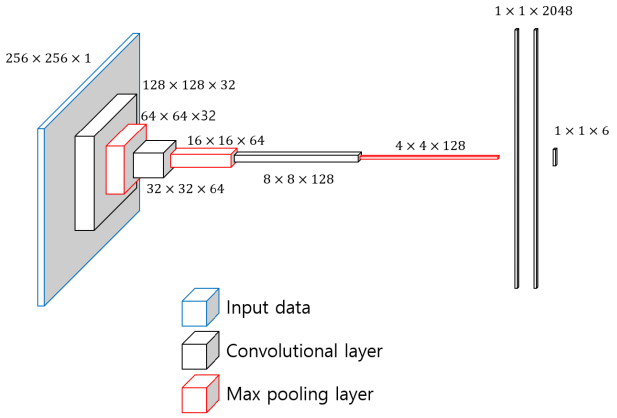

FIGURE 6. The structure of the proposed CNN model.

TABLE 2. The detailed description of CNN model.

Layer	Size of Feature Map	Size of Filters
Input image	256 × 256 × 1	
Conv	128 × 128 × 32	5 × 5 × 32
Batch norm	128× 128 × 32	
ReLU activation	128 × 128 × 32	
Max pooling	64 × 64 × 32	2 × 2
Conv	32 × 32 × 64	5 × 5 × 64
Batch norm	32 × 32 × 64	
ReLU activation	32 × 32 × 64	
Max pooling	16 × 16 × 64	2 × 2
Conv	8 × 8 × 128	5 × 5 × 128
Batch norm	8 × 8 × 128	
ReLU activation	8 × 8 × 128	
Max pooling	4 × 4 × 128	2 × 2
Fully connected	1 × 1 × 2048	
Dropout	1 × 1 × 2048	
ReLU activation	1 × 1 × 2048	
Fully connected	1 × 1 × 2048	
Dropout	1 × 1 × 2048	
ReLU activation	1 × 1 × 2048	
Fully connected	1 × 1 × 6	
Softmax	1 × 1 × 6	
Output	1 × 1 × 6	

This final max pooling layer is followed by fully connected layers. Dropout layers are used after each fully connected layer to prevent overfitting [19]. At the output layer, the output for K classes is obtained using a softmax activation function, as follows:

$$\mathbf{z} = [z_1, \cdots, z_K]^T = \sigma(\mathbf{h}), \tag{19}$$

where z_k is the predicted interference representing the kth category in the K classes, $\mathbf{h} = [h_1, \cdots, h_K]^T$ is the output of the last fully connected layer, and $\sigma(\mathbf{h})$ is the softmax function, which is defined as

$$z_k = [\sigma(\mathbf{h})]_k = \frac{e^{h_k}}{\sum_{i=1}^{K} e^{h_i}}. \tag{20}$$

The mini batch size is set to 256, the learning rate is set to 10^{-4}, and the epoch is set to 10 for training.

C. NETWORK OPTIMIZATION

The parameters for the CNN model are learned through training dataset $\mathcal{T}$ to minimize the loss function. Based on the cross-entropy, the loss function for the jth training sample is calculated as

$$Loss(\mathbf{z}^{(j)}) = -\sum_{k=1}^{K} t_k^{(j)} \log(z_k^{(j)}), \tag{21}$$

where $t_k^{(j)} = 1$ when k is the index for the ground truth of the jth training sample and $t_k^{(j)} = 0$ otherwise. The total loss for the training set is calculated as

$$\mathcal{J}(\Theta) = \frac{1}{|\mathcal{T}|} \sum_{j \in \mathcal{T}} Loss(\mathbf{z}^{(j)}), \tag{22}$$

where Θ represents all learnable parameters for the CNN model and $|\cdot|$ is the number of elements in a set.

To minimize the loss function, several variants of the gradient-descent method have been studied in the literature, such as AdaGrad, AdaDelta, Adam, and momentum [20]. These optimizers adaptively change the learning rate to properly minimize the loss function. Here, we used the momentum optimizer in our experiments.

IV. CLASSIFICATION OF INTERFERENCE SIGNAL

A. SIMULATION ENVIRONMENT

We evaluated the performance of the proposed method through simulation. As mentioned in Section II-B, the ego-vehicle transmits radar signals to detect the target vehicle in front. The interference vehicle drives in the opposite lane and transmits the interference signals. The distance between the detection and target vehicles varied from 10 m to 70 m. The distance between the detection and interference vehicles was also set to vary from 10 m to 70 m. The range of the relative velocity between the detection and target vehicles was set to vary from -30 m/s to 30 m/s. In the case of relative velocity between the detection and interference vehicles, the velocity was set from -60 m/s to 0 m/s.

The parameters of the detection and interference vehicles are presented in Table 3. These system parameters are determined to meet the radar specifications that vary depending on the environment in which the radar is used. For example, the maximum detectable range is expressed as $\frac{cN}{4BW}$ and the velocity resolution is expressed as $\frac{c}{2f_cM\Delta T}$. The values of N and M are usually determined as a power of 2 with a value ranging from 128 to 512, which are set to 256 in this paper.

TABLE 3. Parameters setting of simulation.

Modulation type		Parameter	Value
Ego-vehicle	Fast chirp FMCW	Center frequency	76.5 GHz
		Bandwidth	500 MHz
		Sweep time	10 μs
		# of samples	256
		Sampling frequency	25.6 MHz
		# of chirps	256
Interference vehicle	Unmodulated CW	Center frequency	76.5 GHz
	Slow chirp FMCW	Center frequency	76.5 GHz
		Bandwidth	700 MHz
		Sweep time	1 ms
	Fast chirp FMCW	Center frequency	76.5 GHz
		Bandwidth	800 MHz
		Sweep time	11 μs
	Pulsed CW	Center frequency	76.5 GHz
		Pulse duration	5 μs
		Pulse repitition time	15 μs
	FSK	Center frequency	76.5 GHz
		Bandwidth	600 MHz
		# of steps	17
		Frequency step	37.5 MHz
		Step duration	6 μs

We set $K = 6$ classes for classification: one class for the case when only the target signal was received and five classes for the five different modulations. For convenience, we set each class name as follows: "TS" for target signal, "UC" for unmodulated CW radar signal, "SC" for slow chirp FMCW radar signal, "FC" for fast chirp FMCW radar signal, "PC" for pulsed CW radar signal, and "FSK" for FSK radar signal. We generated 10,000 received signals per class and transformed them into $\mathbf{X}_k^{in}$. 70% of the data was used for training, 15% was used for validation, and 15% was used for test. There are several causes of noise in the radar systems, but the most dominant noise is the thermal noise generated by the radar antenna [19]. Thus, to model the noise of the signal, we assumed the noise to be additive white Gaussian noise (awgn) and set signal-to-noise ratio to 10 dB.

In addition, as all signal post-processing should be performed within a signal period of several tens of milliseconds, an efficient and fast signal processing algorithm is required [23]. Therefore, we also trained the CNN model using a small amount of data to reduce the amount of computation. The conceptual diagram is shown in Fig. 7. We selected chirps to be used from the first column of the time-domain signal matrix $\mathbf{S}$. At this time, if the chirp is taken less, the computational operations in the conversion to 2D range-Doppler response get reduced. We analyzed the accuracy of the model by reducing the number of chirps used and attached the corresponding results.

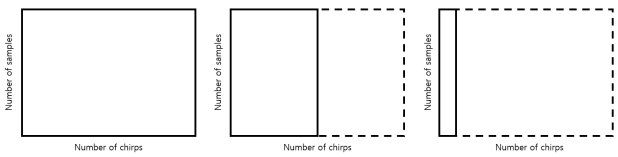

FIGURE 7. Concept diagram showing the use of a small number of chirps.

B. CLASSIFICATION RESULT

We first verified the performance of the CNN model by varying the number of chirps used. The horizontal axis of Fig. 8 represents the number of chirps used for classification. With the proposed method, we can classify the modulation of interference signal with an accuracy over 96%. The use of only 1% of data for the algorithm enables the classification by the CNN model with an accuracy of 96.8%. This is because even if the number of chirps used is reduced, the characteristics of the signal can be seen in the frequency-domain. Therefore, considering a saving of data storage and fast decision, the task can be performed with considerably less chirps. However, for the selection of the number of chirps used, there is a trade-off between the computational cost and the classification accuracy. Using less chirps results in poor performance because the characteristics in frequency-domain get lost. As the number of chirps used increases, the frequency characteristics become more obvious, so the performance increases. When using 8% of the total data (20 chirps), the performance converges to 100%, which can be interpreted as sufficient to represent the frequency characteristics of the interference signal. Therefore, we can conclude that it is better to use at least 8% of the data to ensure classification performance. Less chirps may be used depending on the purpose.

A training progress when using 20 chirps is shown in Fig. 9. The training accuracy, validation accuracy, training loss and

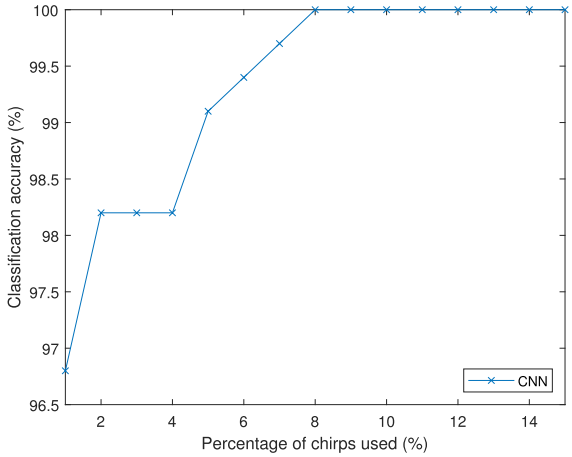

FIGURE 8. Classification accuracy.

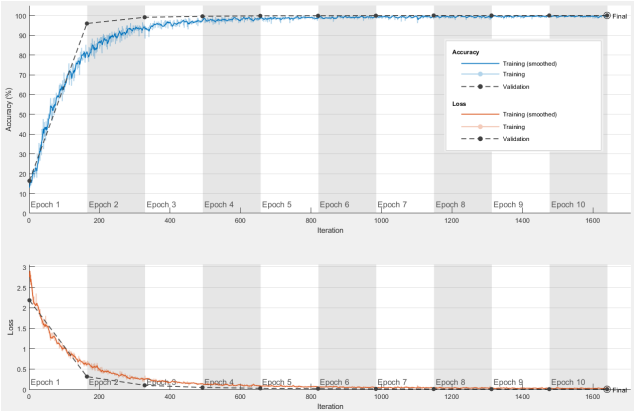

FIGURE 9. Training and validation accuracy and loss when using 20 chirps.

validation loss over epoch number are plotted. As the learning progressed, the accuracy increased and the loss decreased. Finally, the training accuracy and the validation accuracy converged to 100%. Also, because the training loss and the validation loss showed similar tendency, we can say that the model was prevented from over-fitting. Therefore, the model was well trained to classify the interference signals.

Furthermore, we compared the performance of the model with the methods suggested in [8], [9], which used an SVM for classification. The results are shown in Table 4. For comparison, we selected the percentage of chirp used as 8% (20 chirps), which provided a classification performance of 100% for the first time. Compared to two conventional interference classification methods, our proposed method had a better performance. Summarizing the results of Fig. 8 and Table 4, our model is more suitable for interference classification than the conventional methods even when the number of chirps used is small.

We also compared the computational complexities of the three methods in quantitative way. Because the three methods used different classification model, it is hard to strictly compare the complexity. We analyzed the relative complexities through the execution times of them. These times are measured with a MATLAB 2019a program on a computer with an

TABLE 4. Performance comparison when 20 chirps used.

Method	Accuracy	Training time	Test time
Proposed CNN method	100%	350 s	45.8 ms
SVM method in [8]	75.9%	309 s	20.5 ms
SVM method in [9]	94.4%	2,339 s	11.4 ms

AMD Ryzen Threadripper 2990WX 32-Core Processor running at 3.0 GHz. As shown in Table 4, our proposed method took longer time to train than the SVM method in [8] using a linear kernel. However, the training was completed in less time than the method of [9] using a quadratic kernel. When comparing the test time, the results of the three methods are similar in tens of milliseconds.

In addition, we verified the performance of the proposed model using 3% of entire chirps (7 chirps), and the result is shown in Fig. 10. As shown in the figure, most of the test samples were well classified, but some data in classes "TS" and "SC" were misclassified. As shown in Fig. 5, the data in class "SC" do not have dominant patterns of vertical stripes unlike other interference signals. We observed that when the number of chirps used is small, part of the samples in class "SC" is similar to those of class "TS" with noise. We also found that this tendency gradually disappeared as the number of chirps used for classification increased.

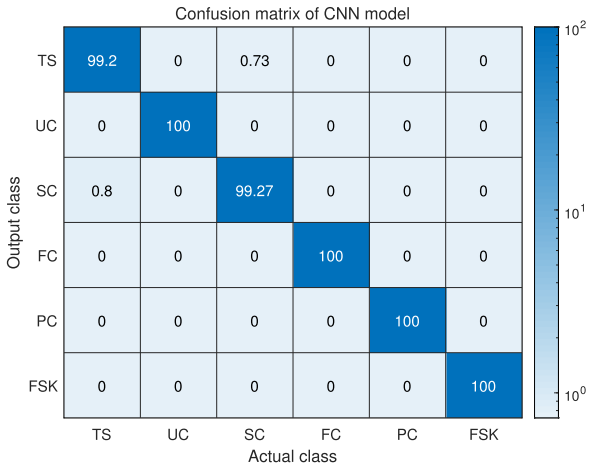

FIGURE 10. Confusion matrix when 7 chirps used.

Fig. 11 represents data visualization using t-stochastic neighbor embedding (t-SNE), which uses stochastic probability to achieve dimensionality reduction. The algorithm preserves the characteristics of the original data even after the dimension of data is reduced to two or three [24]. Figs. 11(a) and (b) show the results of the input and the feature vector, respectively. As shown in Fig. 11(a), some data of each class are located close to each other, but many are mixed and distributed. When the features extracted through the CNN model are used as inputs to the t-SNE algorithm, as shown in the Fig. 11(b), the data of each class are distributed in

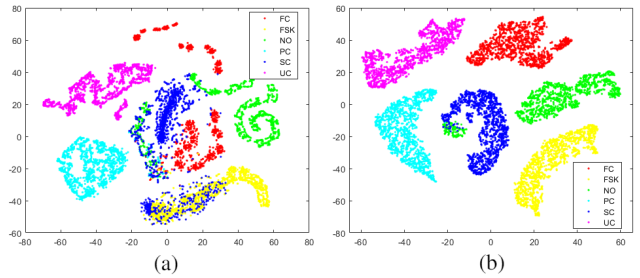

FIGURE 11. Scatter plots of t-SNE algorithm (a) with input data (b) with feature vector.

clusters. Therefore, it is evident that the proposed CNN model appropriately changed the phenotype of the input image for classification.

V. CONCLUSION

In this study, we classified five different modulation types of radar interference signals for automotive radar systems. First, we formulated a mathematical signal model in which the target and the interference signals were received together. Then, using the 2D Fourier transform, these received signals were converted to range-Doppler responses and stored as a set of image data. Finally, we proposed the interference signal classifier using the CNN model based on the generated image data set. We verified that the model identified the modulation type of interference signal with an accuracy of over 96%. In addition, the classification performance of the proposed method was also evaluated using a small number of chirps and it showed more than 5.6%p better performance than the conventional SVM's. Through the proposed method, the modulation types of interference signals from various automotive radar sensors are accurately identified in a short time, so it can be effectively applied to the interference mitigation or interference avoidance. If different mitigation techniques are applied depending on the types of the interference signals, the target detection performance will be greatly increased.

APPENDIX
DERIVATIONS OF MIXER OUTPUT SIGNALS OF INTERFERENCE SIGNALS

In this section, we derived the mixer output signals of five different modulations of interference signals. All the mixer output signals are expressed in one-dimensional time-domain. First, we will express the transmitted signal of the ego-vehicle which uses the fast chirp FMCW radar. Then, signals transmitted from the interference vehicles of five modulation types will be expressed in each subsections. Finally, the transmitted signals from the ego-vehicle and the interference vehicle are mixed considering the round-trip delay t_d and the Doppler shift f_D.

The frequency of the fast chirp FMCW radar system can be expressed as

$$f_{FC}(t) = f_c - \frac{BW}{2} - \frac{BW}{\Delta T}\left(t - m\Delta T\right), \tag{23}$$

where m is the index of chirps. The corresponding transmitted signal can be expressed as

$$S_T(t) = A_T \exp\left(j2\pi\left(\left(f_c - \frac{BW}{2} - mBW\right)t + \frac{BW}{2\Delta T}t^2\right) + j\phi_T\right), \tag{24}$$

where ϕ_T is the initial phase of the signal. This transmitted signal will be multiplied with the transmitted signals of interference vehicles.

A. UNMODULATED CW

The unmodulated CW radar transmits signals with constant frequency. The frequency of this radar can be expressed as

$$f_{UC}(t) = f_{cI}, \tag{25}$$

where f_{cI} is the center frequency of the interference signal. The corresponding transmitted signal can be expressed as

$$S_T(t) = A_T \exp\left(j2\pi f_{cI}t + j\phi_T\right). \tag{26}$$

Then, the received interference signal can be expressed as

$$S_R(t) = A_R \exp\left(j2\pi\left(f_{cI} + f_D\right)\left(t - t_d\right) + j\phi_R\right), \tag{27}$$

where ϕ_R is the initial phase of the received signal. The mixer output signal is obtained by mixing (24) and (27). The corresponding signal can be expressed as Eq. (12).

B. SLOW CHIRP FMCW

The frequency of the slow chirp FMCW radar linearly increases and decreases with time. The frequency of this radar system can be expressed as

$$f_{SC}(t) = f_{cI} - (-1)^{n_S}\frac{BW_I}{2} + (-1)^{n_S}\frac{BW_I}{\Delta T_I}\left(t - n_S\Delta T_I\right), \tag{28}$$

where n_S is the index of the chirps, BW_I is the bandwidth of the interference signal, and ΔT_I is the sweep time of a chirp of the interference signal. The corresponding transmitted interference signal can be expressed as

$$S_T(t) = A_T \exp\left(j2\pi\left(\left(f_{cI} - (-1)^{n_S}\frac{BW_I}{2} - (-1)^{ns}n_S BW_I\right)t + \frac{1}{2}(-1)^{n_S}\frac{BW_I}{\Delta T_I}(t - t_d)^2\right) + j\phi_T\right). \tag{29}$$

Then, the received interference signal can be expressed as

$$S_R(t) = A_R \exp\left(j2\pi\left(\left(f_{cI} - (-1)^{n_S}\frac{BW_I}{2} - (-1)^{ns}n_S BW_I + f_D\right)(t - t_d) + \frac{1}{2}(-1)^{n_S}\frac{BW_I}{\Delta T_I}(t - t_d)^2\right) + j\phi_R\right). \tag{30}$$

The mixer output signal is obtained by mixing (24) and (30). The corresponding signal can be expressed as Eq. (13).

C. FAST CHIRP FMCW

The transmitted signal of the fast chirp FMCW radar is shown in (24). Then, the received interference signal can be expressed as

$$S_R(t) = A_R \exp\left(j2\pi\left(\left(f_{cI} - \frac{BW_I}{2} - m_I BW_I + f_D\right)(t - t_d) + \frac{BW}{2\Delta T}(t - t_d)^2\right) + j\phi_R\right). \quad (31)$$

The mixer output signal is obtained by mixing (24) and (31). The corresponding signal can be expressed as Eq. (14).

D. PULSED CW

In the pulsed CW radar system, the antenna transmits a series of pulses. The frequency of the pulsed CW radar can be expressed as

$$f_{PC}(t) = \sum_{n_P=0}^{N_P-1} f_{cI}\,\mathrm{rect}\left(\frac{t - n_P T_{PRI}}{T_P}\right), \quad (32)$$

where n_P is the index of pulses, N_P is the number of total pulses, rect(·) is a rectangular function, T_{PRI} is the pulse repetition time, and T_P is the pulse duration time. The corresponding transmitted signal can be expressed as

$$S_T(t) = A_T \exp\left(j2\pi \sum_{n_P=0}^{N_P-1} f_{cI}\,\mathrm{rect}\left(\frac{t - n_P T_{PRI}}{T_P}\right) t + j\phi_T\right). \quad (33)$$

Then, the received interference signal can be expressed as

$$S_R(t) = A_R \exp\left(j2\pi\left(\sum_{n_P=0}^{N_P-1} f_{cI}\,\mathrm{rect}\left(\frac{t - n_P T_{PRI}}{T_P}\right) + f_D\right)(t - t_d) + j\phi_R\right). \quad (34)$$

The mixer output signal is obtained by mixing (24) and (34). The corresponding signal can be expressed as Eq. (15).

E. FREQUENCY-SHIFT KEYING

The frequency of this type of modulation varies with discrete values. The frequency of the FSK radar can be expressed as

$$f_{FSK}(t) = f_{cI} - f_{step}\frac{N_{step} - 1 - 2(n_F \bmod N_{step})}{2}, \quad (35)$$

where f_{step} is the frequency difference between two adjacent frequency steps, N_{step} is the number of total frequency steps, and n_F is the index of the step. The corresponding transmitted signal can be expressed as

$$S_T(t) = A_T \exp\left(j2\pi\left(f_{cI} - f_{step}\frac{N_{step} - 1 - 2(n_F \bmod N_{step})}{2}\right) t + j\phi_T\right). \quad (36)$$

Then, the received interference signal can be expressed as

$$S_R(t) = A_T \exp\left(j2\pi\left(f_{cI} - f_{step}\frac{N_{step} - 1 - 2(n_F \bmod N_{step})}{2} + f_D\right)(t - t_d) + j\phi_R\right). \quad (37)$$

The mixer output signal is obtained by mixing (24) and (37). The corresponding signal can be expressed as Eq. (16).

REFERENCES

[1] J. Dickmann, J. Klappstein, M. Hahn, N. Appenrodt, H.-L. Bloecher, K. Werber, and A. Sailer, "'Automotive radar the key technology for autonomous driving: From detection and ranging to environmental understanding,'" in *Proc. IEEE Radar Conf. (RadarConf)*, Philadelphia, PA, USA, May 2016, pp. 1–6.
[2] W. D. Jones, "Keeping cars from crashing," *IEEE Spectr.*, vol. 38, no. 9, pp. 40–45, Sep. 2001.
[3] S. Heuel, "Automotive radar interference test," in *Proc. 18th Int. Radar Symp. (IRS)*, Prague, Czech Republic, Jun. 2017, pp. 1–7.
[4] S. Lee, J.-Y. Lee, and S.-C. Kim, "Mutual interference suppression using wavelet denoising in automotive FMCW radar systems," *IEEE Trans. Intell. Transp. Syst.*, early access, Dec. 13, 2019, doi: 10.1109/TITS.2019.2961235.
[5] J. Jung, S. Lim, J. Kim, S.-C. Kim, and S. Lee, "Interference suppression and signal restoration using Kalman filter in automotive radar systems," in *Proc. IEEE Int. Radar Conf. (RADAR)*, Washington, DC, USA, Apr. 2020, pp. 726–731.
[6] F. Uysal and S. Sanka, "Mitigation of automotive radar interference," in *Proc. IEEE Radar Conf. (RadarConf)*, Oklahoma City, OK, USA, Apr. 2018, pp. 0405–0410.
[7] K.-J. You, H.-E. Jeon, and H.-C. Shin, "Radar modulation identification using inequality measurement in frequency domain," *IEICE Trans. Fundamentals Electron., Commun. Comput. Sci.*, vol. 100, no. 4, pp. 975–981, Apr. 2017.
[8] R. Zhang and S. Cao, "Support vector machines for classification of automotive radar interference," in *Proc. IEEE Radar Conf. (RadarConf)*, Oklahoma City, OK, USA, Apr. 2018, pp. 366–371.
[9] J. Kim, S. Lee, and S.-C. Kim, "Modulation type classification of interference signals in automotive radar systems," *IET Radar, Sonar Navigat.*, vol. 13, no. 6, pp. 944–952, Jun. 2019.
[10] E. A. Hadhrami, M. A. Mufti, B. Taha, and N. Werghi, "Ground moving radar targets classification based on spectrogram images using convolutional neural networks," in *Proc. 19th Int. Radar Symp. (IRS)*, Bonn, Germany, Jun. 2018, pp. 1–9.
[11] A. Palffy, J. Dong, J. F. P. Kooij, and D. M. Gavrila, "CNN based road user detection using the 3D radar cube," *IEEE Robot. Autom. Lett.*, vol. 5, no. 2, pp. 1263–1270, Apr. 2020.
[12] N. Odegaard, A. O. Knapskog, C. Cochin, and J.-C. Louvigne, "Classification of ships using real and simulated data in a convolutional neural network," in *Proc. IEEE Radar Conf. (RadarConf)*, Philadelphia, PA, USA, May 2016, pp. 1–6.
[13] X. Zhou, L.-C. Qian, P.-J. You, Z.-G. Ding, and Y.-Q. Han, "Fall detection using convolutional neural network with multi-sensor fusion," in *Proc. IEEE Int. Conf. Multimedia Expo Workshops (ICMEW)*, San Diego, CA, USA, Jul. 2018, pp. 1–5.
[14] V. Winkler, "Range Doppler detection for automotive FMCW radars," in *Proc. Eur. Radar Conf.*, Munich, Germany, Oct. 2007, pp. 1445–1448.
[15] A. Krizhevsky, I. Sutskever, and G. E. Hinton, "Imagenet classification with deep convolutional neural networks," in *Proc. Adv. Neural Inf. Process. Syst. (NIPS)*, 2012, pp. 1097–1105.
[16] S. Ioffe and Z. Christian, "Batch normalization: Accelerating deep network training by reducing internal covariate shift," in *Proc. 32nd Int. Conf. Mach. Learn.*, Lille, France, 2015, pp. 448–456.
[17] V. Nair and G. E. Hinton, "Rectified linear units improve restricted Boltzmann machines," in *Proc. 27th Int. Conf. Mach. Learn.*, Haifa, Israel, Jun. 2010, pp. 1–8.
[18] A. Giusti, D. C. Ciresan, J. Masci, L. M. Gambardella, and J. Schmidhuber, "Fast image scanning with deep max-pooling convolutional neural networks," in *Proc. IEEE Int. Conf. Image Process.*, Melbourne, VIC, Australia, Sep. 2013, pp. 4034–4038.

[19] N. Srivastava, G. Hinton, A. Krizhevsky, I. Sutskever, and R. Salakhutdinov, "Dropout: A simple way to prevent neural networks from overfitting," *J. Mach. Learn. Res.*, vol. 15, no. 1, pp. 1929–1958, 2014.
[20] S. Ruder, "An overview of gradient descent optimization algorithms," 2016, *arXiv:1609.04747*. [Online]. Available: http://arxiv.org/abs/1609.04747
[21] N. Qian, "On the momentum term in gradient descent learning algorithms," *Neural Netw.*, vol. 12, no. 1, pp. 145–161, 1999.
[22] M. A. Richards and J. K. Author, *Fundamentals of Radar Signal Processing*, 2nd ed. New York, NY, USA: McGraw-Hill, 2014, pp. 41–100.
[23] A. D. C. Gmbh, "ARS 408-21 premium long range radar sensor 77 GHz," Continental, Hanover, Germany, Tech. Rep., Version 04, 2015.
[24] L. van der Maaten and G. Hinton, "Visualizing data using t-SNE," *J. Mach. Learn. Res.*, vol. 9, pp. 2579–2605, Nov. 2008.

JINWOOK KIM (Graduate Student Member, IEEE) received the B.S. degree in electrical and computer engineering from Seoul National University (SNU), Seoul, South Korea, in February 2016. His current research interests include radar signal processing, including improving target detection performance and classifying mutual interference, indoor localization using Wi-Fi signals, and deep learning applications.

SEONGWOOK LEE (Member, IEEE) received the B.S. and Ph.D. degrees in electrical and computer engineering from Seoul National University (SNU), Seoul, South Korea, in February 2013 and August 2018, respectively. From September 2018 to February 2020, he worked as a Staff Researcher with the Machine Learning Laboratory, AI & SW Research Center, Samsung Advanced Institute of Technology (SAIT), Suwon, South Korea. Since March 2020, he has been an Assistant Professor with the School of Electronics and Information Engineering, College of Engineering, Korea Aerospace University, Goyang. He has published more than 50 articles on radar signal processing. His research interests include radar signal processing techniques, such as improved angle estimation, target recognition and classification, clutter suppression, mutual interference mitigation, and target tracking. He also received the Distinguished Ph.D. Dissertation Award from the Department of Electrical and Computer Engineering, SNU.

YONG-HWA KIM (Member, IEEE) received the B.S. degree in electrical engineering and the Ph.D. degree in electrical and computer engineering from Seoul National University, Seoul, South Korea, in 2001 and 2007, respectively. From 2007 to 2011, he was a Senior Researcher with the Korea Electrotechnology Research Institute (KERI), South Korea. From 2011 to 2013, he was an Assistant Professor with the Division of Maritime Electronic and Communication Engineering, Mokpo National Maritime University, South Korea. Since March 2013, he has been the Faculty Member with the Department of Electronic Engineering, Myongji University, South Korea. His research interests include communication systems, fault diagnosis, and digital signal processing. His current research interests include artificial intelligence for communications, radar systems, and smart grid.

SEONG-CHEOL KIM (Senior Member, IEEE) received the B.S. and M.S. degrees from Seoul National University, Seoul, South Korea, in 1984 and 1987, respectively, and the Ph.D. degree from the Polytechnic Institute of NYU, Brooklyn, NY, USA, in 1995, all in electrical Engineering. From 1995 to 1999, he was with the Wireless Communications Systems Engineering Department, AT&T Bell Laboratories, Holmdel, NJ, USA. Since 1999, he has been a Professor with the Department of Electrical and Computer Engineering, Seoul National University. His current research interests include system engineering of wireless communications, including millimeter wave channel modeling, localization algorithms, power line communications, and automotive radar signal processing.